Research article

Multiscale analysis and experimental validation of the effective elastic modulus of epoxy-dioctahedral phyllosilicate clay composite

O.O. Daramola [a,d,*], J.L. Olajide [b], A.A. Adediran [c], B.O. Adewuyi [a], T.T. Ayodele [a], D.A. Desai [b], E.R. Sadiku [d]

[a] Department of Metallurgical and Materials Engineering, Federal University of Technology Akure, Nigeria
[b] Department of Mechanical and Automation Engineering, Tshwane University of Technology, Pretoria, South Africa
[c] Mechanical Engineering Department, Landmark University, Omu-Aran, Kwara State, Nigeria
[d] Institute of NanoEngineering Research (INER) and the Department of Chemical, Metallurgical and Materials Engineering, Tshwane University of Technology, Pretoria, South Africa

A R T I C L E   I N F O

A B S T R A C T

In this research, developed finite element codes were used to study the effective elastic modulus and stress-strain distribution profiles of epoxy resin filled with 6 wt. % microparticles of kaolinite. The random distribution of the particles was microstructurally regenerated with Digimat MSC software and random sequential algorithm codes in epoxy matrix. Stochastic representative volume element models of the composites were developed and analyzed under periodic boundary conditions. For validation, the predicted result by finite element analysis was compared with that of Mori-Tanaka's mean field homogenization scheme, selected micromechanical models and experiment. All the results indicated that 6 wt. % of kaolinite microparticles can improve the elastic modulus and load-bearing capacity of epoxy resin with <5 % error between predicted and actual results. The microstructure, phase identification and chemical characterization of the composite were also studied with scanning electron microscopy, x-ray diffraction spectroscopy and energy-dispersive x-ray spectroscopy, respectively. In addition, the particle size and distribution of the kaolinite in the epoxy matrix were experimentally investigated.

1. Introduction

As a result of the attractive properties of epoxy and epoxy composites, their applications and investigations in various commercial sectors and research fields have continued to witness an excessive rise. This is substantially corroborated by the exponential increase in the number of research findings currently associated with their subject matter [1, 2, 3]. Most significantly, the effort of researchers in the areas that are greatly concerned with providing economically viable and effective solutions to the limitations of epoxy resin in service applications such as poor fracture toughness and fair barrier properties [1]. As a result of this exploratory expedition, the experimental campaign to fill epoxy polymers with inorganic inclusions and organic fibres became an active field of research [1, 2, 3]. A large percentage of common inorganic inclusions are naturally occurring clay minerals with ample abundance in nature and promising properties that can be beneficially exploited to override the above-mentioned drawbacks of traditional epoxy [4]. The clay mineral of interest to this study is kaolinite.

Kaolinite belongs to the class of dioctahedral phyllosilicate (serpentine-group) clay minerals. It is an industrial mineral with a chemical formula; $Al_2Si_2O_5(OH)_4$ and a triclinic crystal system [5]. It is a stratified silicate mineral of which the strata are held together by hydrogen bonds with one tetrahedral sheet of silica linked through oxygen atoms to one octahedral sheet of alumina octahedral [6]. It is well known for its large abundance in nature, low shrink-swell capacity, ion exchange capacity, chemical resistance, thermal stability, flame retardancy and excellent barrier properties [5, 6, 7]. By virtue of these attractive properties, it has become an eye-catching reinforcing material for the development of Polymer Matrix Composites (PMCs) [5, 6, 7].

Many researchers have reported the positive influence of kaolinite addition to PMCs. Su et al. [8] reported improved thermal stability, brittle-to-ductile fracture mode and water-resistant property of epoxy resin nanocomposites filled with 3–10 wt. % functionalized kaolinite inclusions. Elimat et al. [9] demonstrated that filling polycarbonate with 5–10 wt. % kaolinite-silica micro-inclusions resulted in enhanced thermal conductivity of the developed composites with increasing

* Corresponding author.
E-mail addresses: oodaramola@futa.edu.ng, jimmylolu@gmail.com, dladesoji@gmail.com (O.O. Daramola).

experimental temperature. According to Al-Ramadin *et al.* [10] the AC electrical conductivity and dielectric constant of polycarbonate-kaolinite composites increased with increasing micro-sized kaolinite content (5–15 wt. %) in the polycarbonate matrix. Mon *et al.* [11] have also reported excellent improvement in the tensile properties of Ethylene Propylene Diene Monomer (EPDM) rubber-(1–7 wt. %) kaolinite nanocomposites produced by solution intercalation. Introduction of 2–10 wt. % annealed kaolinite particles into polytetrafluoroethylene (PTFE) matrix also resulted in favourable increase in the wear resistance of the PTFE-kaolinite composites [12]. Similarly, de Macédo Neto *et al.* [13] successfully improved the wear resistance of polystyrene nanocomposites reinforced with 1–3 wt. % kaolinite particles.

From the studies mentioned in the preceding paragraph, it is obvious that kaolinite is a suitable choice of reinforcement for PMCs, most especially in little quantity. However, most researchers concentrated on modified kaolinite/nano-sized kaolinite inclusions as their choice of reinforcement in PMCs and this explicitly clarifies why there has been a dwindling interest in raw micro-sized kaolinite as reinforcements in PMCs [8, 9, 10, 11, 12]. In addition, previous findings have shown the limitations of raw kaolinite as reinforcement in PMCs due to some of its unappealing intrinsic properties such as absence of intercalated charge-balancing cations and linkage of its adjacent layers by hydrogen bonds. The latter is responsible for the difficulty associated with functionalizing kaolinite surfaces which usually results in poor dispersion of kaolinite inclusions in various polymer matrices [8].

Attempts made by researchers to eliminate these drawbacks include mechanical, thermal, chemical and thermochemical modifications of kaolinite particles prior to or during their deployment in PMCs, however the associated rise in cost and reduced eco-integrity of the resultant composites cannot be pushed aside [8, 9, 10, 11, 12]. As a result of this, adoption of cost-effective, fast and dependable numerical frameworks for virtual characterization of new materials began to gain significant attention. Examples of these numerical approaches include Finite Element Analysis (FEA) [14], molecular dynamics simulation [15], quantum chemical/mechanical calculations [16] and statistical modeling [17].

In this research, efforts were made to predict the Effective Elastic Modulus (EEM) and Stress-Strain Distribution Profile (SSPD) of Epoxy/Kaolinite Composite (EKC), 3-Dimensional Representative Volume Element (3DRVE) models and FEA were employed. An RVE model is an infinitesimal part of the system under study which is projected to be large enough to be a true representative of the constituent media [18]. It is important to mention at this point that experimental investigation of the above-mentioned properties might constitute a big challenge in terms of financial implications, labour-intensiveness and time constraint since repeatability of experiment is vital to increase the confidence level of experimental results [19]. In addition, the visualization and detailed understanding of SSPDs in composites are easier with results obtained from FEA-3DRVE models than in experimental results. A detailed and very interesting investigation by Omairey *et al.* [20] shows the capabilities of 3DRVE models in realistic representation of heterogenous materials and also numerical homogenization of the 3DRVE models by FEA using Periodic Boundary Conditions (PBCs).

In computational continuum mechanics, the primary goal of numerical homogenization is to compute macroscopic properties from microscopic properties. Numerical homogenization is an efficient way to determine the effective properties such as elastic modulus and thermal conductivity of periodic composite materials [21]. Numerical homogenization can be first-order homogenization or second-order homogenization. The first-order homogenization is based on the asymptotic expansion theory and the methods of averages. In this approach, the deformation gradient tensor is used to solve the problem at the micro scale and then the macroscopic stress tensor is obtained using the averaging equation. As for the second-order homogenization, the deformation gradient tensor and the Lagrangian gradient are used to solve a value boundary problem (a system of ordinary differential equations with

solution and derivative values specified at more than one point) at the micro scale. This approach permits the solution of macro scale problem in the presence of moderate localization, as macroscopic deformation gradients are transferred to the RVE boundaries [22].

Although, most of the reported findings have proven to be worthwhile, it was found out that most of the authors developed their RVE models via traditional approaches such as Voronoi Tessellation [23], Random Sequential Adsorption (RSA) algorithm [24] and Monte Carlo simulation [14]. Some of these approaches are sometimes cumbersome, intricate and time-consuming (might require learning of new programing language(s) with steep learning curve(s)). Consequently, this becomes a problem where rapid and dependable predictions of effective properties of composite materials are required [25].

On the bright side, this can be easily taken care of with Python Programming Language (PPL) or Digimat multiscale modeling software package (Digimat). With reference to Digimat, this software automatically takes care of the numerical homogenization, applications of PBCs, mesh convergence, RVE convergence and computation of desired results. Hence, it offers fast prediction of composites' effective properties at reduced computational cost, power and time. The reliability and accuracy of Digimat-FE tool in predicting the effective properties of composite materials using the FEA-RVE approach is available in the work of Orban *et al.* [26].

In the present study, the effect of adding 6 wt. % raw kaolinite with particle size of 1.9087 µm to epoxy resin on the EEM of the resultant EKC was investigated. The prediction of EMM and SSPDs of prepared EKCs were done with FEA-3DRVE modeling using Digimat-FE tool. The result from Digimat-FE was validated by predictions of Digimat-MF, selected micromechanical models, PPL-MATLAB-RSA-generated 3DRVE models (solved by FEA codes in ABAQUS software) and experimental results. 6 wt.% was chosen as the preferable volume fraction for kaolinite as previous findings have shown it is apparently the critical filler content beyond which elastic modulus of polymer-kaolinite composites begins to drop [8, 11]. This has been attributed to the high tendency of raw kaolinite particles to agglomerate at this filler content unless they are subjected to surface modification [8, 11, 12].

2. Materials and methods

2.1. Materials

Bisphenol A diglycidyl ether epoxy resin (DGEBA commercial grade) and epichlorohydrin and triethylenetetramine were the constituents of the matrix used in this study. This matrix was procured from Orkila Chemicals, Ikeja, Lagos State, Nigeria. The raw kaolinite used as the reinforcing phase of the composites was sourced and collected from Ikere-Ekiti clay deposit, in Ekiti State, Nigeria. The properties of both materials from the supplier and literature [27] are presented in Table 1. Figure 1 shows 3D schematics of the materials.

2.2. Methods

In this research, both numerical and experimental methods were employed for the preferred analysis. The numerical section is divided into different stages as shown in Figure 2.

2.2.1. Mean field homogenization model based on Mori Tanaka Formulation

In the first stage, mean-field homogenization (MFH) prediction was used to determine the EEM of the composite using Digimat-FE software. This approach is based on a non-linear, semi-analytical homogenization theory that offers fast, accurate and efficient predictions at the macroscopic scale (composite level). The results at the microscopic scale (constituent phases) are averaged. With this approach no RVE is generated, the required parameters are the material behaviour of the phases, the microstructural morphology and the mechanical loading. The MFH

Table 1. Properties of the materials used for numerial analysis.

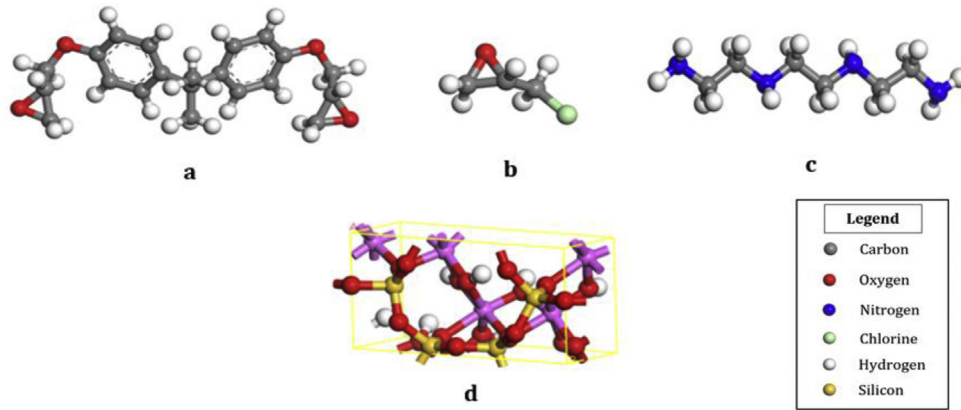| Matrix	Density kg/m^3	Young Modulus MPa	Poisson Ratio	Constitutive Law
Epoxy	1.25×10^3	3 100	0.35	Elastic Isotropic
Inclusion				
Kaolinite	2.65×10^3 [27]	21 400 [27]	0.3 [27]	Elastic [27] Isotropic

Figure 1. 3D schematic representation of (a) Bisphenol A diglycidyl ether (b) Epichlorohydrin (c) Triethylenetetramine (d) kaolinite ((a–c) are matrix materials and (d) is reinforcing material).
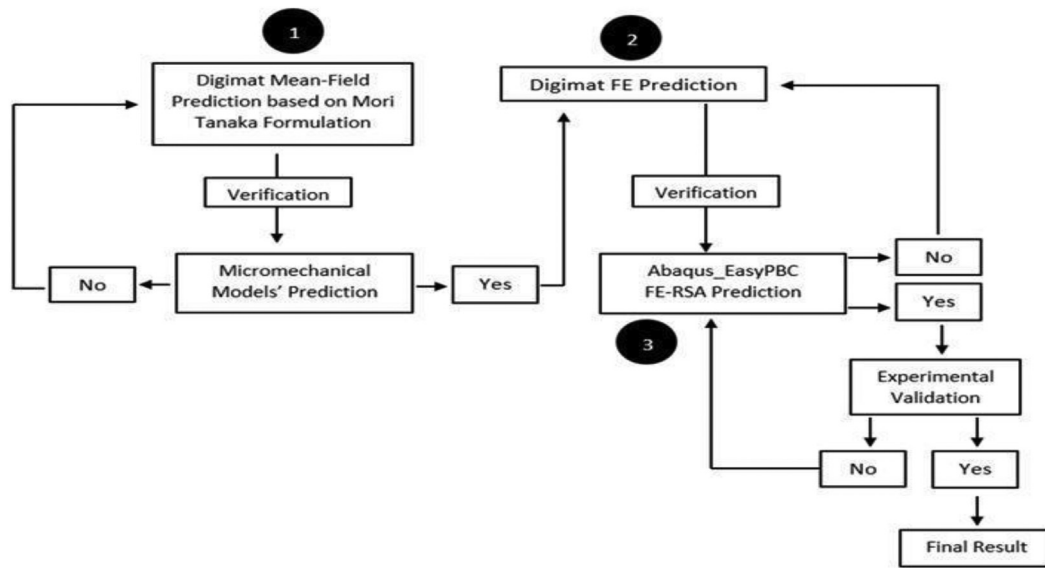

Figure 2. Boolean flowchart of the adopted numerical methodologies featured for prediction and verfication of the EEM of the EKC with the numbers 1, 2 and 3 represnting stage 1, stage 2 and stage 3 of the protocol adpated in this research, respectively.

model's prediction in this research is based on the first order Mori-Tanaka homogenization (MTH) technique [28].

The MFH approach is a fast (requires no generation of RVE model and meshing) and efficient way to forecast the effective elastic properties of linear elastic composites. The mean-field stress (σ) and strain (ε) in each phase I and associated parameters are given in Eqs. (1), (2), (3), (4), (5), and (6) [29]:

$$\overline{\sigma}_J = \langle \sigma \rangle_I \tag{1}$$

$$\overline{\varepsilon}_J = \langle \varepsilon \rangle_{I,} \tag{2}$$

Where

$$\langle f \rangle = \frac{1}{V} \int_V f dV \tag{3}$$

The macro field can be written as

$$\langle * \rangle = v_f^M \langle * \rangle_M + \sum_{I=1}^{N} v_f^I \langle * \rangle_M \tag{4}$$

Where.

v_f^M is the volume fraction of the matrix phase and v_f^I is the volume fraction of the inclusion phase. For the single inclusion case, if all the constituents are linear elastic, the strain in the inclusion is linked to the strain in the matrix through a concentration tensor A.

$$\langle \in \rangle_I = A \langle \in \rangle_M \tag{5}$$

The MTF assumes that each inclusion acts like a lonely attachment and the strain in the matrix is considered as the far-field strain. Therefore, the concentration tensor can be written as:

$$A = \left[E : \left(C_M^{-1} C_I - I \right) + I \right]^{-1} \tag{6}$$

Where "E" is the Eshelby Tensor, "C_M" is the stiffness of the matrix and "C_I" is the stiffness of the inclusion.

2.2.2. Micromechanical model

For verification of the MFH model's prediction, micromechanical models were employed to verify the accuracy of the model prior to the FEA. The micromechanical models used for verification are stated in Eqs. (7), (8), (9), (10), (11), (12), and (13) [19].

2.2.2.1. Rule of mixture model.
For micro-particle-reinforced polymer composites where the particles restrain the deformation of the matrix if well bonded, the rule of mixtures can be utilized to forecast the elastic modulus of the composite [19]. Eqs. (7) and (8) show the upper and lower bound predictions, respectively. With respect to filler volume fraction for particulate composites, Eqs. (7) and (8) can be translated into the Voight and Reuss models, respectively [19].

$$E_c = E_m V_m + E_f V_f \tag{7}$$

$$E_c = \frac{E_m E_f}{E_f V_m + E_m V_f} \tag{8}$$

Voight model

$$E_c = V_f E_f + \left(1 - V_f\right) E_m \tag{9}$$

Reuss model

$$\frac{1}{E_C} = \frac{V_f}{E_f} + \frac{\left(1 - V_f\right)}{E_m} \tag{10}$$

Where "E_c", "E_m" and "E_f" are Young's modulus values of the composite, matrix and filler/particulate, respectively. Also, "V_m" and "V_f" correspond to the volume fractions of the matrix and filler, respectively.

Halpin-Tsai model.
The Halpin and Tsai model has been extensively used for the prediction of elastic modulus of polymers filled with different types of inclusion geometries. The model is:

$$\frac{E_c}{E_m} = \frac{1 + \cap \vartheta V_f}{1 - \cap V_f} \tag{11}$$

$$\cap = \frac{E_f/E_m - 1}{E_f/E_m + \vartheta} \tag{12}$$

Where "ϑ" corresponds to the shape factor which is dependent on the geometry of the inclusion. For spherical inclusion it is given as 1.25 [19].

Kerner's model

$$E_C = E_m \left(1 + \left(\frac{15(1 - v_m)V_f}{(8 - 10 v_m)V_m} \right) \right) \tag{13}$$

Valid for $E_f \gg E_m$ and where "v_m" corresponds to Poisson ratio of the matrix.

2.2.3. Finite element model development

2.2.3.1. RVE generation.
In continuum mechanics, for statistically homogeneous materials, an RVE is regarded as a picture of the material to be utilized to predict the resultant actual properties of a homogenized macroscopic model with a volume which is minute when likened to the macroscopic body and sufficiently enormous when likened to the microstructural size. RVE models play important part in the mechanism

and dynamics of haphazard dissimilar materials, when forecasting their actual elastic properties [14, 22, 23, 24].

In this research, 3DRVE models for the FEA were automatically generated by Digimat-FE and RSA algorithm with MATLAB codes and python scripts. The RVE models generated via RSA and python scripts were based on the method in the work of Kiran [30]. The radius of the particle was taken as 0.99035 μm and the RVE size was kept at least twice the diameter of the inclusion.

2.2.3.2. Boundary conditions and mesh.
For the 3DRVE models generated with Digimat-FE, they were subjected to pre-defined PBCs and mechanical loading in Digimat and for the RVE models generated with RSA algorithm, they were subjected to EasyPBC plugin PBCs and mechanical loading in ABAQUS CAE [20]. The mesh type used for the Digmat-FE was conforming tetra (5 refinement steps) with quadratic elements, internal coarsening, curvature control and choral deviation ratio of 1.5. Similarly, quadratic tetrahedral element (CD310) was used for the RSA-3DRVE model in ABAQUS. Different 3DRVEs with different sizes were developed and the best 3DRVE size L^3 with values of elastic modulus closest to the MFH model's prediction was selected for further analysis. The total number of elements in the meshed RVEs in both approaches did not exceed 60,000.

2.3. Experimental section

2.3.1. Particle preparation

The kaolinite clay was sourced for and collected from Ikere-Ekiti kaolinite clay deposit, Ikere-Ekiti, Ekiti State, Nigeria located on latitude 7.52009 °N and longitude 5.222 °E with yearly temperature that varies from 290.9 K to 305.38 K and is rarely below 287.59 K or above 308.15 K [31]. The as-collected clay was milled with the aid of a laboratory ball mill and soaked in water for 72 h. The soaked clay sample were vigorously mixed in a clockwise direction with the aid of a ceramic blunger. The resultant mixture was removed from the blunger and packed inside a transparent container and allowed to settle (sedimentation method of separating clays into different particle sizes) [32]. Four different layers were observed namely colloids, very fine, fine and coarse particle sizes. The clay samples were separated accordingly and allowed to dry for 4 weeks at room temperature of $27 \pm 2\,°C$. Dried clay samples were manually pulverized with the aid of laboratory mortar and pestle. The 6 wt. % kaolinite used for this research was obtained from the very fine particle size. The same particle size was taken to the laboratory for particle size analysis, phase identification and chemical characterization. This was ensued by introduction of the kaolinite inclusion into epoxy matrix for composite development and characterization. The schematic representation of the clay preparation is presented in Figure 3.

2.3.2. Composites development

The composites based on preferred combination of epoxy resin, pulverized kaolinite clay and the hardener were developed using open mould casting technique. The total wt. % of kaolinite used was 6. In order to achieve a homogeneous mixture of the constituents, manual stirring of the mixture was carried out for 3 min. This was ensued by casting the mixture in appropriate tensile test moulds. The test samples were allowed to cure for 24 h in the mould and for another 27 days at room temperature of $27 \pm 2\,°C$ after which they were removed from the moulds. The experimental techniques used for the characterization of the composites include energy dispersive x-ray spectroscopy, x-ray diffraction, scanning electron microscopy and tensile test.

2.3.3. Particle size analysis

To determine the average particle size of the very fine kaolinite particle, particle size analyser was employed. The determinate particle size limit of the apparatus is 0.05–3000 μm and it is fitted with a miniature bulk sample distribution component. A lens limit of 300RF, a beam
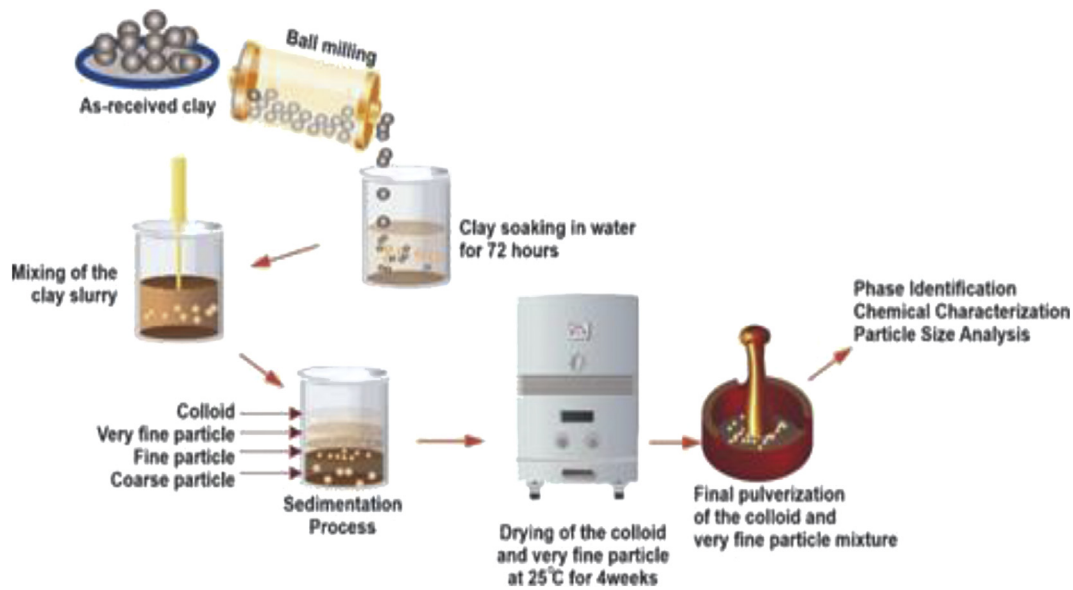
Figure 3. Flowchart of the experimental procedure for kaolinite particle preparation.

interval of 2.4 mm with polydisperse examination was utilized for this measurement. Approximately 0.5 g of kaolinite particles were distributed in deionized water in the sample distribution component of the aparatus, dynamically blended for 2 min at a speed of 2 100 rpm, and sonicated for 45 s. Measurements were taken and the diffraction data graphs were generated.

2.3.4. Powder X-ray diffraction analysis

Structural information and the degree of crystallinity of the kaolinite and the epoxy/kaolinite composite was analysed using a Rigaku Multi-flex powder X-ray diffractometer (Netherlands). The analysis was carried out under the following conditions: wavelength of 0.154 nm using a Cu kα radiation source, a voltage/applied current of 40 kV and 30 mA respectively. The instrument was programed to scan the sample from 10° to 80° (2θ degrees) range with a step of 0.5° θ/minute. The d-spacing, d and lateral crystal size, L, were calculated using Bragg's law equation as shown in Equations (14 -15) [33].

$$d = \frac{\gamma}{2Sin\theta} \tag{14}$$

$$L = \frac{K\gamma}{\beta Cos\theta} \tag{15}$$

Where θ, is the diffraction angle and λ, is the wavelength of the incident radiation which is 0.154nm, K is the structural factor, usually taken as 0.9 for epoxy [33, 34], β is the full width at half maximum.

2.3.5. Tensile test

The tensile test was carried out to ascertain the elastic modulus of the composites with the aid of a universal tensile testing machine (Instron Engineering Corporation USA), 2010 model, with a load cell of 10 kN in accordance with ASTM D638-10 standards (ASTM, 2010) [35]. Dumb bell samples prepared by hand layup technique were tested in tension mode at a single strain rate of 5 mm/min at room temperature of 25 °C and relative humidity of 40 %. The specimen with gauge length 14 mm was fixed on the machine and the machine was switched on. The specimen was fractured and the load-extension graph and elastic modulus data were generated. The final result is the mean value of 6 test samples.

2.3.6. Microstructural examination

The morphology of the composite was examined with the aid of Scanning Electron Microscope (SEM) (Carl Zeiss, Germany) with an accelerating voltage of 15 kV. The samples were mounted on aluminum stubs and were sputter coated prior to the SEM analysis.

3. Results and discussion

3.1. Particle size analysis result

The result of the particle size analysis of the kaolinite (pulverized very fine particle) is presented in Figure 4. This analysis is very important as the definition of particle size and shape factor plays significant role in numerical prediction of the effective properties of the composite materials. The equivalent mean diameter of the particles was found to be 1.9807 μm which was used for the FEM analysis. This is in conformity with the research carried out by Talabi *et al.* [36] whereby they stated the 44.5 wt. % particle size of unpulverized kaolinite (from the same Ikere-Ekiti kaolinite clay deposit) passed through 75 μm sieve and further processing such as intercalation with urea can refine the grain size. Also, according to Heinskanen [37], the grain size of kaolinite ranges from 1–50 μm which is in agreement with this result.
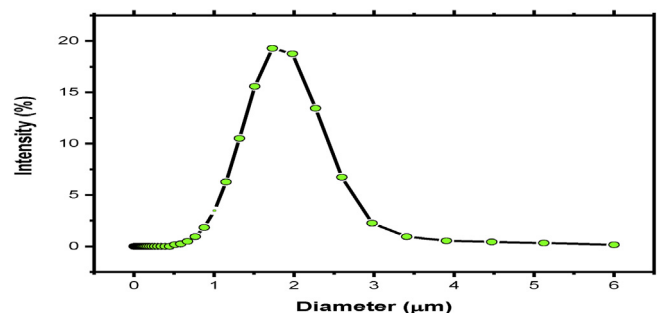

Figure 4. Mean particle size plot of the kaolintie clay.

3.2. XRF result for kaolinite

The chemical composition of the kaolinite inclusion as a function of XRF result is presented in Table 2. The clay was found to consist of six different oxides with SiO_2 having the highest composition seconded by Al_2O_3. This correlates with what was observed by Elimat *et al.* [9] for Baten El-Ghoul kaolinite clay in Jordan.

3.3. XRD result for kaolinite and the epoxy/kaolinite composites

The XRD analysis reveal the sample as Kaolinite Clay as shown in Figure 5(a) with chemical formula $Al_2Si_2O_5(OH)_4$ (Aluminum Silicate Hydroxide) which is an inorganic mineral with ICDD number 14-164. The mineralogy of the kaolinite clay as a function of XRD result is presented in Figure 5 and Table 3. The crystal structures of neat epoxy and EKC are presented in Figure 5 (a-b). The Figure revealed an intense peak at $2\theta = 24.67°$ for neat epoxy. However, for 6 wt.% EKC, the ultimate intensity was considerably lowered to $18.18°$. The interparticle -d- spacing slightly increased signifying blended intercalated and little clustering comportment. The diffraction angles and corresponding interparticle -d- spacing and the lateral crystal size for neat epoxy and EKC are presented in Table 3. The table indicates the inter-particle -d- spacing has increased from 0.36 nm for neat Epoxy to 0.47 for 6 wt.% EKC, respectively. This signifies the extent of intercalation of the kaolinite layers in epoxy matrix. Nevertheless, it has been established that at higher than 6 wt.% kaolinite, the kaolinite inclusions may become problematic to disperse and incomplete exfoliation and insertion of these inclusions occurred [35]. This is as a result of the sturdy propensity of kaolinite inclusions to cluster at higher weight fractions ˃ 8 wt. % [34], so the lateral crystal size increased from 1.47 nm for neat epoxy to 2.65 nm for the epoxy/kaolinite composite.

3.4. EDX result of kaolinite and epoxy/kaolinite composite

The EDX spectra and the quantitative results of the minerals present in the kaolinite, and the epoxy/kaolinite composite is presented in Figure 6/Table 4 and Figure 7/Table 5, respectively.

Observations from Figure 6 -EDX spectrum of kaolinite revealed that the predominant elements in the kaolinite are Al, Si and O as indicated by their peaks on the spectrum. This result is in agreement with the XRF result of kaolinite where alpha quartz (SiO_2) is the predominant mineral (85.92 %). Akinyemi *et al.* [31] have reported a similar finding. However, the quantitative result also revealed that this mineral is highly rich in iron which is also in conformity with the research carried out by Sengupta *et al.* [39].

Observations from Figure 7 -EDX spectrum of the epoxy/kaolinite composite revealed peaks of elements that are typically dominant in epoxy resin (C and O for Epoxy) and kaolinite clay (Al, Si and O for Kaolinite). This is anticipated for a composite made of both materials. The close peak values of the predominant constituents of each material somewhat translates to a satisfactory homogeneous mixture.

3.5. SEM image and image analysis results

The digitally processed SEM images results of the EKC {Figure 8 (a-b)} and the as-received SEM image of the EKC {Figure 8(c)} are presented in Figure 8. From the results, it was observed that the particles are evenly distributed in the epoxy matrix. Also, there are no notable sites of debonded particles in the epoxy matrix. This is a clear indication that in the absence of coupling agents, the content of available matrix in the composite is sufficient to strongly bond with the total volume of the inclusions used as reinforcement. Similar results have been presented by

researchers with 1–7 wt. % kaolinite in some polymer matrices [11, 12, 13]. The observed distribution aided the development of the 3DRVE model without clustering effect. Besides, clustering effect are more pronounced for nanoparticles which is not the case in the present study [38].

3.6. Finite element results and discussion

In Figure 9, the result of the effective elastic properties of the EKC predicted by Digimat-FE is presented. From the results, it was perceived that the EEM of the composite improved by 143.5 MPa in comparison with that of the neat epoxy. The maximum equivanlent Von Mises Stress and the maximum principal total strain were found to be 240.534 MPa and 0.0582826, respectively. This increment in the elastic modulus of the composite is credited to the stiffness of kaolinite (21 000 MPa) being higher than that of the epoxy matrix (3100 MPa) and the succesful transmission of the applied load from the ductile epoxy matrix to the more rigid filler. The latter mechanism can be clealry seen in Figure 9 as the maximum stress regions (red parts) are more pronounced on the fillers. This discovery is in comformity with the findings of Mon *et al.* [11] wherein they filled EPDM rubber with 1–7 wt.% kaolinite inclusions. Similarly, Sleptsova *et al.* [12] reported maximum increase of elastic modulus of PTFE filled 5 wt.% kaolinite inclusion. Moreover, this improvement is expected as the enhancement in the stiffness of a composite material is not dependent on the bonding strength between the filler and matrix. This factor is preeminently critical for enhancement in tensile strength of particulate-filled polymer matrix [11, 12].

More importantly, FEA allows the easy visualization of the magnitude of load bore by each phase of the composite. This one of the important factors that makes FEA a consequential tool in the virtual characterization of composite materials for engineering applications.

In Figure 10, the predicted effective elastic properties of the epoxy matrix, the kaolinite inclusion and the EKC by ABAQUS-PYTHON-MATLAB based on RSA algorithm are presented. Similarly, the result showed that the EEM of the composite increased by 147.84 MPa. This is in good agreement with the prediction of Digimat FE which shows the reliability of the two approaches. It was also found that, the equivalent Von Mises Stress and the maximum principal strain of the matrix also increased with the addition of the inclusion. The equivlalent Von Mises Stress of the matrix increased from 620 MPa to 3848 MPa while the strain increased from 0.1792 to 0.5711.

The SSPDs across the neat epoxy, the kaolinite inclusion and the EKC can be seen in Figure 10. The neat epoxy exhibited the minimum stress and strain values while the kaolinite and EKC exhibited the same maximum stress values. Interestingly, the maximum strain value was observed for the EKC. This is an indication that the volume fraction of the inclusion used simultneously increased the stiffness and the strain-to-fracture of the composite. Tilbrook *et al.* [39] have reported a similar enhancement when they reinforced epoxy with particles of alumina.

More importantly, it was found that there was no significant increase in the density of the neat epoxy with the addition of 6 wt. % kaolinite inclusion. The observed increment was <0.01. This is a good indication in terms of contemporary application as the demand for low density materials with improved performance is currently on a steep rise [1, 2, 3].

3.7. Empirical validation by micromechanical models

Figure 11 and Table 6 show the validation results of the predictive methods and their % errors, respectively. It was found that the closest value to the experimental result was given by the prediction of the Reuss's model. However, this method will not be selected as it does not take into

Table 2. Chemical composition of kaolinite.

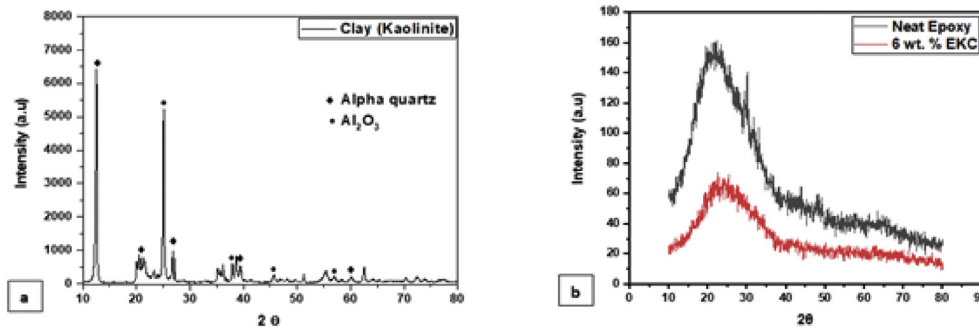| Compound	Al_2O_3	SiO_2	SiO_2	CaO	CaO	Fe_2O_3	ZrO_2	Na_2O	MgO
Weight %	35.64	55.90	2.33	0.83	1.56	2.44	0.31	0.41	0.46

Figure 5. XRD result of (a) Kaolinte clay and (b) epoxy/kaolinite clay composite.

Table 3. Diffraction angle and the corresponidng interparticle -d- spacing and lateral crystal size of the neat epoxy and the EKC.

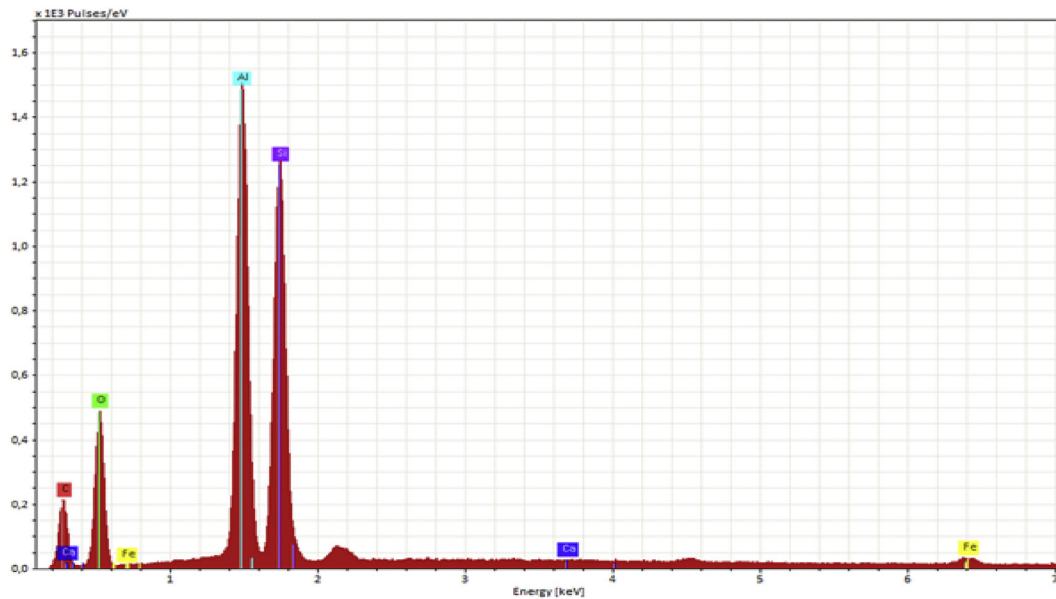| Sample designation	2θ (°)	β (radian)	θ (radian)	d (nm)	L (nm)
Neat Epoxy	24.670	0.096	0.215	0.360	1.480
6wt.% Epoxy/Kaolinite Composite	18.176	0.0531	0.164	0.472	2.646

Figure 6. EDX result of the kaolinite clay.

Table 4. Quantitative EDX result of the kaolinite clay.

LCE

Element	At.No	Netto	Mass [%]	Mass Norm. [%]	Atom [%]	abs.error [%]	rel.error [%] (1 sigma)
Oxygen	8	33289	27.32	32.81	34.42	3.36	12.28
Carbon	6	13421	26.19	31.44	43.95	3.55	13.55
Aluminium	13	127827	15.82	18.99	11.82	0.78	4.95
Silicon	14	116864	13.37	16.05	9.60	0.60	4.46
Iron	26	2960	0.58	0.70	0.21	0.04	7.66
Calcium	20	46	0.01	0.01	0.00	0.00	15.73
		Sum	83.29	100.00	100.00		

account many vital parameters such as inclusion geometry, inclusion size and distribution of the inclusion in the matrix [19]. Asides, the predictions observed for the Kerner's model and the Voight's model, there exists great correlations between the results of the remaining four predictive models namely, Halpin-Tsai, Meanfield, Digimat-FE and FEA-RVE-RSA/ABAQUS and that of experimental modulus with <5 % error. A similar error range has been reported by Drugan and Willis [40] in a similar investigation. In comparison with the experimental results, all of the models overpredicted the EEM of the composites. This can be associated with the fact the numerical composites are assumed to be
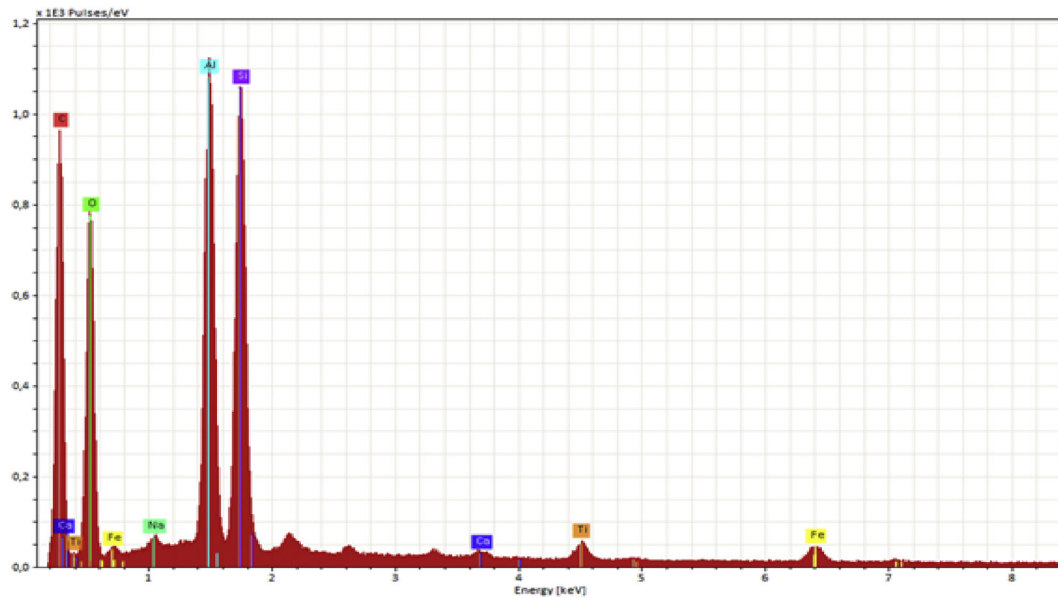
Figure 7. EDX result of the EKC.

Table 5. Quantitative EDX result of the EKC.

LCE

| Element	At.No	Netto	Mass [%]	Mass Norm. [%]	Atom [%]	abs.error [%]	rel.error [%] (1 sigma)
Carbon	6	62301	40.17	47.83	58.97	4.69	11.66
Oxygen	8	53827	29.30	34.89	32.29	3.46	11.81
Aluminium	13	93108	6.37	7.58	4.16	0.33	5.19
Silicon	14	96542	5.76	6.86	3.62	0.27	4.71
Calcium	20	1710	0.21	0.25	0.09	0.03	15.87
Iron	26	5500	1.08	1.29	0.34	0.06	5.36
Titanium	22	5044	0.78	0.93	0.29	0.05	6.40
Sodium	21	2320	0.31	0.37	0.24	0.05	15.37
	Sum		83.99	100.00	100.00		
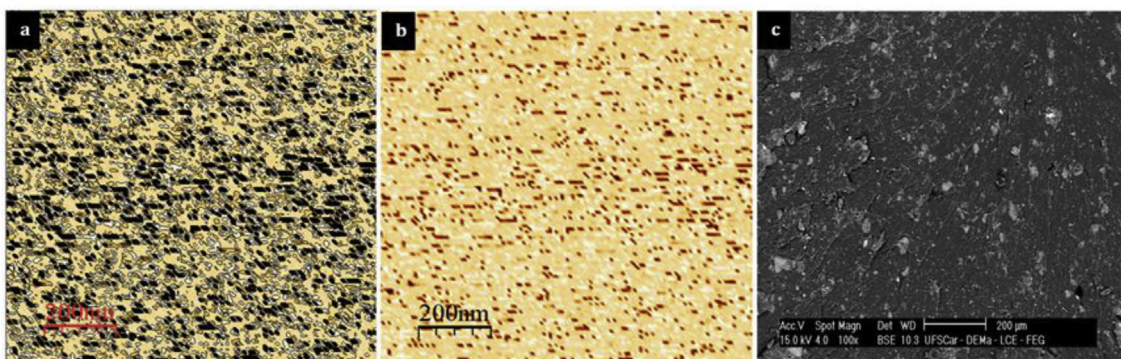
Figure 8. (a–b) Digitally processed SEM images results of the EKC and (c) As-Received SEM image of the EKC.

ideally elastic isotropic which is hardly the case for true experimental materials. Factors, such as manufacturing defects and averaging of different results from repeatability experiments might contribute to the observed discrepancy between the experimentally observed and the predicted results. In addition, the elastic modulus value of 21 000 MPa assigned to the kaolinite for numerical study was gotten from literature [27]. It is possible that the true value in reality (maybe dependent on location) is lower than this which in turn will further explain the

observed discrepancy between the predicted and experimental results. Experiments are encouraged in this regard for clarification. More importantly, similar cases have been reported by some researchers [41]. Ultimately, the predictive accuracy of the models can be described as semi-quantitative relative to the comparison between the experimental error of 3.5 % from 6 repeatability tests and mean average error of the models' predictions which is 4.23 % (excluding Voight's upper bound prediction treated as an outlier). Relative to real life scenario, the
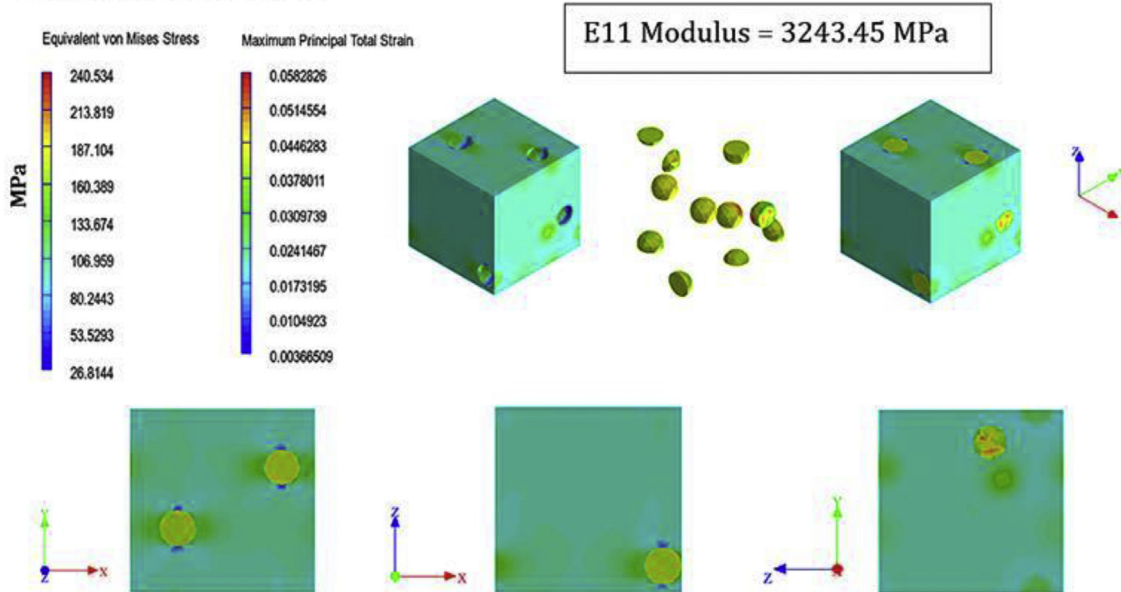
Digimat FE prediction

Figure 9. Finite element results of the predicted effective elastic properties of the EKC with Digimat-FE.
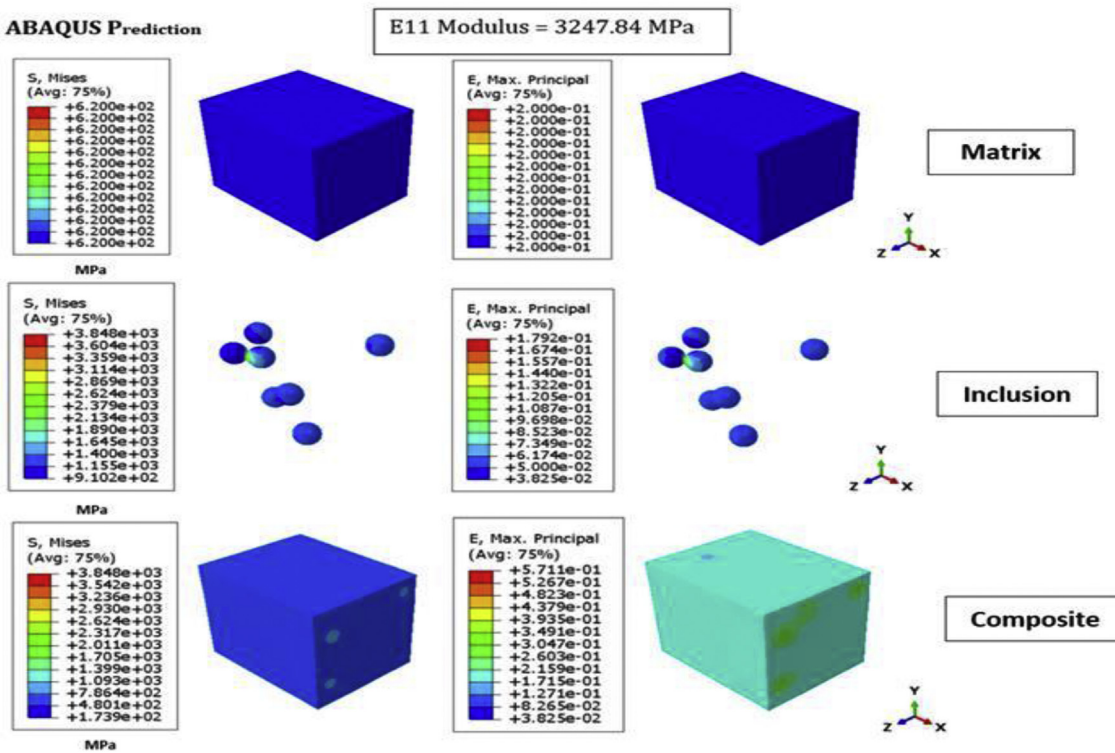

Figure 10. Finite element results of the predicted effective elastic properties of the neat epoxy, kaolinite inclusion and the EKC with ABAQUS-PYTHON-MATLAB based on RSA algorithm in the x-direction.

risk/safety factor associated with the design concept and area of applications of the material will be the principal determinant of permissible error [41]. For more accurate predictions, parametric study that will feature factors such as inclusion geometry irregularities, interparticle distance and probable cluster effect amongst others should be considered. More importantly, it is believed that the implementation of this parametric protocol will shift the predictive accuracy of the models towards a more quantitative zone.

E11 Modulus = 3243.45 MPa

4. Conclusions

The influence of 6 wt. % micro-sized kaolinite particle on the EEM of epoxy polymer matrix composite has been numerically investigated and experimentally validated. The following conclusions were drawn:
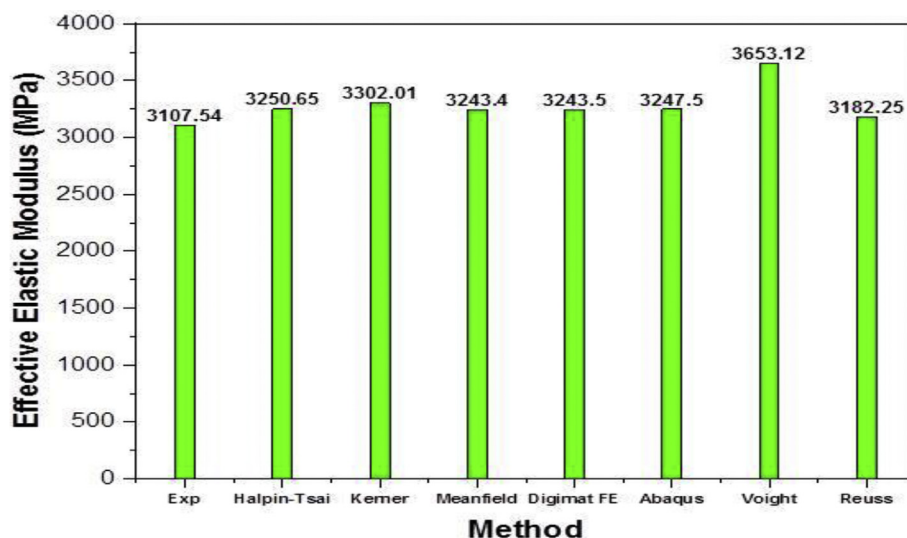
Figure 11. Validation results for the predicted elastic modulus of the EKC.

Table 6. % Error of each predictive method in comparison with the experimental result.

Method	Values	% Error (in comparison with the experimental result)
Experimental	3107.5	3.5
Halpin-Tsai	3250.6	4.4
Kerner	3303	5.9
Mean Field	3243.4	4.2
Digimat FE	3243.5	4.2
Abaqus	3247.5	4.3
Voight	3634.4	14.5
Reuss	3182.3	2.4

- The SSDPs indicated efficient stress transfer from the matrix to the fillers resulting in enhanced load-bearing capacity of the EKC in comparison with the monolithic polymer
- Experimental elastic modulus of the composite increased from 3100 MPa to 3107.54 MPa. However, close values but greater improvements were observed for the predicted effective elastic moduli by all the featured models. This is a clear indication that in the case of near-perfect experimental conditions, greater improvement might be feasible. On the other hand, more influencing factors that were not considered in the present study can be incorporated into the models for near–perfect replication of the experimental setup.
- The discrepancy between the prediction of the modeling approaches (Digimat-FE 3DRVE model and RSA-generated 3DRVE model subjected to EasyPBC PBC) and the experimental result is ultimately <5 %. This shows that both approaches are reliable, however, since the Digimat-FE requires lesser computational resources and time in comparison with the RSA approach, it will be a better option.
- The MFH prediction is also reliable. However, it does not show the stress-strain distribution profiles of the composite.
- The discrepancy between the predicted and experimental results may be due to the assumed perfect spheres and a single particle size for the inclusions. The authors hope to look into this effect with an icosahedron geometry and a particle

Declarations

Author contribution statement

O. O. Daramola, J. L. Olajide: Conceived and designed the experiments; Analyzed and interpreted the data; Wrote the paper.

A. A. Adediran: Analyzed and interpreted the data; Wrote the paper.

B. O. Adewuyi: Contributed reagents, materials, analysis tools or data; Wrote the paper.

D.A. Desai: Contributed reagents, materials, analysis tools or data.

T. T. Ayodele: Performed the experiments.

E. R. Sadiku: Contributed reagents, materials, analysis tools or data.

Competing interest statement

The authors declare no conflict of interest.

Additional information

No additional information is available for this paper.

References

[1] J.S. Jayan, A. Saritha, K. Joseph, Innovative materials of this era for toughening the epoxy matrix: a review, Polym. Compos. 39 (54) (2018) E1959–E1986.

[2] N.R. Paluvai, S. Mohanty, S. Nayak, Synthesis and modifications of epoxy resins and their composites: a review, J. Polym-Plast Technol. Eng. 53 (16) (2014) 1723–1758.

[3] N. Saba, M. Jawaid, O.Y. Alothman, M. Paridah, A.J. Hassan, Recent advances in epoxy resin, natural fiber-reinforced epoxy composites and their applications, J. Reinforc. Plast. Compos. 35 (2016) 447–470.

[4] J.Z. Liang, Reinforcement and quantitative description of inorganic particulate-filled polymer composites, Compos. B Eng. 51 (2013) 224–232.

[5] C. Detellier, S. Letaief, Kaolinite–Polymer Nanocomposites, Developments in Clay Science. Handbook of Clay Sci, Elsevier, 2013, pp. 707–719.

[6] J.E. Gardolinski, L.C.M. Carrera, M.P. Cantao, F. Wypych, Layered polymer-kaolinite nanocomposites, J. Mater. Sci. 35 (2000) 3113–3119.

[7] Y.X. Jia, L.J. Sun, X.G. Chen, M. An, X.M. Sang, A review on polymer/kaolinite nanocomposites, Adv. Mater. Res. Trans. Tech. Publ. (2013) 213–216.

[8] L. Su, X. Zeng, H. He, Q. Tao, S. Komarneni, Preparation of functionalized kaolinite/epoxy resin nanocomposites with enhanced thermal properties, Appl. Clay Sci. 148 (2017) 103–108.

[9] Z.M. Elimat, A.M. Zihlif, G. Ragosta, Optical and thermal properties of polycarbonate/kaolinite composites, J. Thermoplast. Compos. Mater. 23 (6) (2010) 793–805.

[10] Y. Al-Ramadin, A.M. Zihlif, Z.M. Elimat, G. Ragosta, Dielectric and AC electrical conductivity of polycarbonate kaolinite composites, J. Thermoplast. Compos. Mater. 22 (2009) 617–632.

[11] S.G. Mon, Y.J.V. Ruban, D.V. Roy, Synthesis of kaolinite-filled EPDM rubber composites by solution intercalation: structural characterization and studies on mechanical properties, Appl. Nanosci. 1 (2011) 131–135.

[12] S. Sleptsova, S. Laukkanen, N. Gladkina, V. Fedoseeva, A. Okhlopkova, L. Grigoryeva, Effect of kaolinite on the properties and structure of PTFE, in: AIP Conference Proceedings, AIP Publishing, 2018, 040092.

[13] J.C. de Macèdo Neto, R. Botan, L.M.F. Lona, J.E. Neto, W.A. Pippo, Polystyrene/kaolinite nanocomposite synthesis and characterization via in situ emulsion polymerization, Polym. Bull. 72 (2015) 387–404.

[14] H. Ahmadi Moghaddam, P. Mertiny, Stochastic finite element analysis framework for modelling mechanical properties of particulate modified polymer composites, Materials 12 (17) (2019) 2777.

[15] X. Zhang, H. Wen, Y.J.P. Wu, Computational thermomechanical properties of silica–epoxy nanocomposites by molecular dynamic simulation, Polymers 9 (2017) 430.

[16] S. Khostavan, M. Fazli, M.G. Ahangari, Y. Rostamiyan, The effect of interaction between nanofillers and epoxy on mechanical and thermal properties of nanocomposites: theoretical prediction and experimental analysis, Adv. Polym. Technol. (2019) 1–10.

[17] S. Feli, M.M. Jalilian, Experimental and optimization of mechanical properties of epoxy/nanosilica and hybrid epoxy/fiberglass/nanosilica composites, J. Compos. Mater. 50 (28) (2016) 3891–3903.

[18] D. Jeulin, T. Kanit, S. Forest, Representative volume element: a statistical point of view, in: D.J. Bergman, E. Inan (Eds.), Continuum Models and Discrete Systems. NATO Science Series (Series II: Mathematics, Physics and Chemistry), 158, Springer, Dordrecht, 2004, pp. 21–27.

[19] O.O. Daramola, J.L. Olajide, S.O. Babarinsa, E.R. Sadiku, Rutile titania-filled polyethylene composites: microstructural evolution, empirical modeling of the mechanical properties and comparative validation of the quasi-elastic modulus using micromechanical models, Fibers Polym. 19 (2018) 1347–1358.

[20] S.L. Omairey, P.D. Dunning, S. Sriramula, Development of an ABAQUS plugin tool for periodic RVE homogenisation, J. Eng. Comp. 35 (2019) 567–577.

[21] E. Andreassen, C.S. Andreasen, How to determine composite material properties using numerical homogenization, J. Computa. Mater. Sci. 83 (2014) 488–495.

[22] J. Yvonnet, Computational Homogenization of Heterogeneous Materials with Finite Elements. Solid Mech. And its Appli, Springer Nature Switzerland, 2019, p. 258.

[23] J. Alsayednoor, P. Harrison, Evaluating the performance of microstructure generation algorithms for 2-d foam-like representative volume elements, Mech. Mater. 98 (2016) 44–58.

[24] L. Chen, B. Gu, Zhou, Development of the RSA method for random short fiber reinforced elastomer composites with large fiber aspect ratios, Mater. Res. Express 6 (6) (2019), 065322.

[25] S. Bargmann, B. Klusemann, J. Markmann, J.E. Schnabel, K. Schneider, C. Soyarslan, J. Wilmers, Generation of 3D representative volume elements for heterogeneous materials: a review, Mater. Sci. 96 (2018) 322–384.

[26] Y.A. Orban, D.L. Manea, C. Aciu, Study of methods for simulating multiphase construction materials, Proc. Manufac. 22 (2018) 256–261.

[27] N.H. Mondol, J. Jahren, K. Bjørlykke, I. Brevik, Elastic properties of clay minerals, Lead. Edge 27 (6) (2008) 758–770.

[28] W. Ogierman, G. Kokot, Mean field homogenization in multi-scale modelling of composite materials, J. Achiev. Mater. and Manufac. Eng. 61 (2) (2013) 343–348.

[29] abaqus-docs.mit.edu. https://abaqusdocs.mit.edu/2017/English/SIMAC AEMATRefMap/simamat-c-meanfieldhomogenization.htm, 2017. (Accessed 23 December 2019).

[30] R. Kiran, Thermal conductivity of polymer composites filled with nanofillers, Preprints (2016).

[31] S.A. Akinyemi, S.O. Ogunniyi, A.O. Ojo, W.M. Gitaric, A. Momoh, O.O. Akinola, A.O. Talabi, L.O. Afolagboye, O.A. Olaolorun, O.S. Ayodele, Mineralogy, physicochemical characteristics and industrial potential of some residual clay deposits within Ekiti state, southwestern Nigeria, J. Environ. Earth Sci. (2014) 70–88.

[32] I.C. Bernhardt, in: first ed.Particle Size Analysis: Classification and Sedimentation Methods. Part. Tech. Series, Springer Sci. & Business Media, Springer Netherlands, 2012, 978-94- 011-1238-3.

[33] S. Dolati, A. Fereidoon, A.R. Sabet, Hail impact damage behaviors of glass fiber reinforced epoxy filled with nanoclay, J. Compos. Mater. 48 (10) (2014) 1241–1249.

[34] M. Murugan, V. Kokate, M.J. Bapat, Synthesis, characterization and evaluation of reflectivity of nanosized cation/epoxy resin composites in microwave bands, Bull. Mater. Sci. 34 (2011) 699.

[35] ASTM D638–10, Standard Test Method for Tensile Properties of Plastics, American Society for Testing and Materials, West Conshohocken, PA, 2010.

[36] A.O. Talabi, O.L. Ademilua, O.O. Akinola, Compositional features and industrial application of Ikere kaolinite, southwestern Nigeria, Res. J. Eng. Appl. Sci. 1 (5) (2012) 327–333.

[37] K. Heinskanen, in: first ed.Particle Classification, Particle Technology Series, Springer, Netherlands, 1993, 978-0-412-49300-3.

[38] P. Sengupta, P.C. Saikia, P.C. Borthakur, SEM-EDX characterization of an iron- rich kaolinite clay, J. Sci. Ind. Res. 67 (2008) 812–818.

[39] M. Tilbrook, R. Moon, A.E. Hoffman, On the mechanical properties of alumina–epoxy composites with an interpenetrating network structure, Mater. Sci. Eng. 393 (2005) 170–178.

[40] W. Drugan, J.R. Willis, A micromechanics-based non local constitutive equation and estimates of representative volume element size for elastic composites, J. Mech. Phys. Solid. 44 (4) (1996) 497–524.

[41] C.R. Chen, S.Y. Qin, S.X. Li, J.L. Wen, Finite element analysis about effects of particle morphology on mechanical response of composites, Mater. Sci. Eng. 278 (1-2) (2000) 96–105.